Rev.Adv.Mater.Sci. 25 (2010) 168-175

MECHANICAL PROPERTIES AND MICROSTRUCTURE EVOLUTION DURING DEFORMATION OF ULTRAFINE GRAINED ZIRCONIUM AT LOW TEMPERATURES

E. D. Tabachnikova[1], A. V. Podolskiy[1,2], B. Bonarski[2], C. Mangler[2], V. Z. Bengus[1], S.N. Smirnov[1], A. N. Velikodny[3], M. A. Tikhonovsky[3] and M. J. Zehetbauer[2]

[1]B. Verkin Institute for Low Temperature Physics & Engineering, NASU, Lenin Ave. 47, Kharkov, 61103, Ukraine
[2]Physics of Nanostructured Materials, Faculty of Physics, University of Vienna, Boltzmanngasse 5, A-1090 Wien, Austria
[3]National Science Center "Kharkiv Institute of Physics and Technology", Academicheskaya St. 1, Kharkov, 61108, Ukraine

Received: December 10, 2009

Abstract. Mechanical properties of ultrafine grained (UFG) zirconium (grain size 200 nm), produced by a combination of extrusion, wire drawing and specific annealing, were studied at temperatures 4.2 – 300K in uniaxial compression and compared with coarse grained (CG) Zr. In parallel, investigations by X-ray diffraction (texture) and transmission electron microscopy were undertaken in order to reveal the evolution of the microstructure with increasing strain. Volume fractions of twins have been determined for UFG and CG Zr. It has been found that the activity of twinning is smaller in UFG Zr in comparison with CG Zr at ambient and lower temperatures, but the contrary is true for very low temperatures (4.2K), where twinning increases with decreasing grain size. The influence of twinning on mechanical properties of UFG Zr has been discussed, too.

1. INTRODUCTION

In recent years, the ultrafine grained (UFG) state (grain size < 1 μm) was produced not only in face-centered cubic (fcc) but also hexagonal closely packed (hcp) metals, such as Zr and Ti, by several methods of severe plastic deformation (SPD) [1], such as equal-channel angular pressing [2,3], accumulative roll-bonding [4], and others. The average grain size achieved using various SPD techniques lies in the range 150-300 nm. The investigation of mechanical properties in a wide temperature range of the materials after SPD has shown considerable increase of strength while with maintaining a rather good level of plasticity [5,6]. A further quite promising method of production of UFG zirconium, consisting of combination of extrusion, thermal treatment and wire drawing, was suggested in our previous work [7].

While there has been some progress in studying the mechanical properties of ultrafine grained hcp metals, questions remain concerning the evolution of microstructure during straining, which determine the mechanical characteristics observed. This is especially true for deformation at low tempera-

Corresponding author: Aleksey V. Podolskiy, e-mail: podolskiy@ilt.kharkov.ua

tures, where twinning – in addition to dislocation gliding mechanism of plasticity – should be active.

Thus, the aim of this work is to study the mechanical properties and the concomitant evolution of microstructure by means transmission electron microscopy (TEM) and X-ray diffraction (XRD) methods of UFG Zr at low temperatures. The UFG structure was achieved in Zr by a combination of extrusion, thermal treatment and wire drawing. This method is similar to that used in [7], but with some improvements, which allowed to additionally increase the strength of UFG Zr by approximately 30 % in comparison with the results of [7].

2. EXPERIMENTAL MATERIALS AND METHODS

Polycrystalline zirconium subjected to double electron-beam melting served as the experimental material. The average grain size in the initial ingots was 1–2 mm, and the total impurity content was about 0.1 wt.%, including 0.05% hafnium, 0.01% carbon, 0.07% oxygen, and 0.01% iron. The residual resistivity of the material was $\rho_{293}/\rho_{4.2} \approx 40$. Ingots with 50 mm in diameter were extruded to rods with 10 mm at 775K, which resulted in the formation of 0.4 мм large grains (the true extrusion strain has been 4.1). Severe plastic straining of the rods was performed by wire drawing at room temperature down to diameters 3 mm without intermediate annealing (the true wire drawing strain has been 2.4). Afterwards, the rods were ground and chemically polished and then cut by spark erosion into 2.5 mm in diameter and 5 mm high cylindrical samples for mechanical compression tests. The cylinder axis was also the direction of the $<10\bar{1}0>$ axis of the texture arising in zirconium rods during wire drawing (c-axis of crystallites preferably oriented perpendicularly to the cylinder axis). Then, these UFG samples were annealed at 575K for 3 h to decrease the density of free lattice defects. A part of the samples was annealed at 850K for 1 h to produce coarse grained (CG) structures with grain sizes of about 10 μm. The microstructure of the sample was studied in terms of longitudinal and transverse sections using a TESLA BS-613 transmission electron microscope. The microstructure of the UFG samples being subjected to different strains by uniaxial compression at different temperatures was studied in transverse sections with a Philips CM200 transmission electron microscope operated at an acceleration voltage of 200 kV. For TEM specimen preparation, discs of 0.5 mm thickness were cut from the samples by spark erosion and mechanically ground to a thickness of about 0.15 mm. Then, discs were electropolished to perforation using an electrolyte consisting of 5% perchloric acid and 95% ethanol at temperature -20 °C.

TEM photographs were investigated by statistical analysis methods from which grain size distribution functions were determined.

The mechanical characteristics of UFG and CG Zr samples were studied at 300, 170, 77, and finally at 4.2K by recording the load-time curves for samples compressed along the sample axis with relative strain rate $5 \cdot 10^{-4}$ s^{-1} in an MRK-3 deformation machine (stiffness $7 \cdot 10^6$ N/m). The registered curves were converted into stress-plastic strain diagrams $\sigma(\varepsilon)$ on which the conventional yield stress $\sigma_{0.2}$, and the maximum achieved stress σ_f and strain ε_f were determined. The quantity σ was determined as the ratio of the load to the initial cross-sectional area of a sample, and the value of ε was calculated as the ratio of the change of the length of a sample due to plastic strain to its initial length. With the aim of study the evolution of microstructure samples were compressed at temperatures 300, 170, 77, and 4.2K till the following values of strain: 0.02, 0.06, 0.12, and 0.18.

Texture measurements of initial and strained samples were performed by means of a high resolution Bruker-AXS D 8 X-Ray diffractometer in combination with a 2D detector, using Cu Kα radiation. The beam was collimated to a spot size of 500 mm. The Orientation Distribution Function (ODF) has been calculated using the Arbitrary Defined Cells (ADC) method [8] with LABOTEX 3.0 texture analysis software [9]. Textures were measured at the centre of sample surface normal to compression (= sample) axis, after having removed the surface layers (0.5 mm) by mechanical grinding. Pole figures $(10\bar{1}0)$, (0001), $(10\bar{1}1)$, and $(10\bar{1}2)$ have been registered. Pole figures $(10\bar{1}0)$ and (0001) were used for analysis of texture changes in samples subjected to different degrees of strain by uniaxial compression at different temperatures.

3. EXPERIMENTAL RESULTS

3.1. Microstructure of initial UFG samples (after extrusion, wire drawing, and annealing)

Electron microscopy of the UFG samples showed that microstructure is rather uniform. Fig. 1a shows the microstructure in the transverse section of the samples. Grains of 0.1-0.4 μm in size can be seen, and the interior of the grains is nearly free from dis-

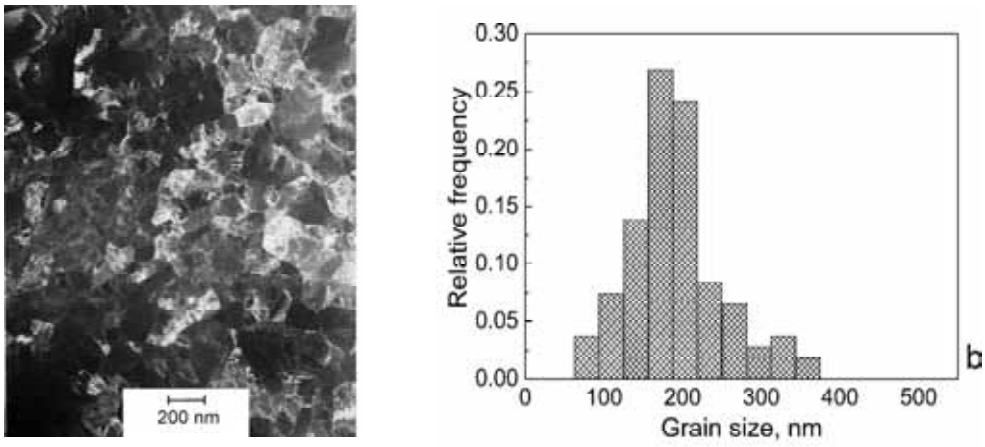

Fig. 1. (a) TEM image of transverse section of the specimen in the UFG structural state; (b) histogram of the grain size distribution - data from several images.

location pileups, grain boundaries are rather clear and straight, which is typical of an annealed structure. A histogram of the grain size distribution in the transverse section of the samples is displayed in Fig. 1b. From the histogram the most likely size of the grains is calculated as about 0.2 μm. A striped structure typical of wire drawing and extrusion, i.e. grains elongated in the direction of the wire drawing axis, is observed in the longitudinal section of the samples.

3.2. Mechanical properties of the UFG Zr

Fig. 2 shows the temperature dependence of the yield stress $\sigma_{0.2}$ for the UFG structural state of Zr and also for the CG one. It can be seen from Fig. 2 that at all temperatures studied, values of $\sigma_{0.2}$ for UFG state are approximately 2.4-3 times larger than for the CG samples, due to decrease of the average grain size from 10 to 0.2 μm. In both structural states of Zr studied, an increase of $\sigma_{0.2}$ values with decreasing compression temperature was registered, as well as an increase of temperature dependence of yield stress, which is typical of thermally activated plasticity. The only exception is the UFG state at 4.2K which exhibits approximately the same yield stress as that observed at 77K.

Typical deformation curves of UFG and CG states of Zr are shown in Fig. 3. Several features of the plastic strain process can be noted: (i) for all temperatures and structural states studied, a decrease of temperature leads to an increase of strength at any point of the deformation curves; (ii) serrated plastic flow occurs at a temperature of 4.2K, which is typical of such low temperature for many metals

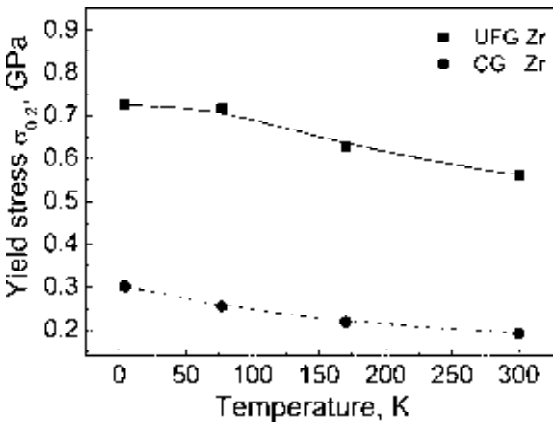

Fig. 2. Temperature dependence of the yield stress of Zr in UFG and CG state (experimental errors are less than the size of points in the plot).

and alloys including CG Zr; (iii) several stages at deformation curves of UFG and CG Zr are observed.

In contrast to stress-strain curves, plots of the hardening rate $\Theta(\varepsilon)=d\sigma/d\varepsilon$ as function of compression strain much better exhibit characteristic 'stages' of plastic deformation for UFG and CG Zr samples (Fig. 4), (for compression test at 4.2K, the strain hardening coefficients were calculated from an approximation curve, which combines the maxima of stress serrations). The deformation stages have been denoted A, B, C which is consistent with definition suggested previously [10] for the description of strain hardening in compression of CG hexagonal metals.

Two main stages at the strain dependence of the strain hardening coefficient Θ can be seen in

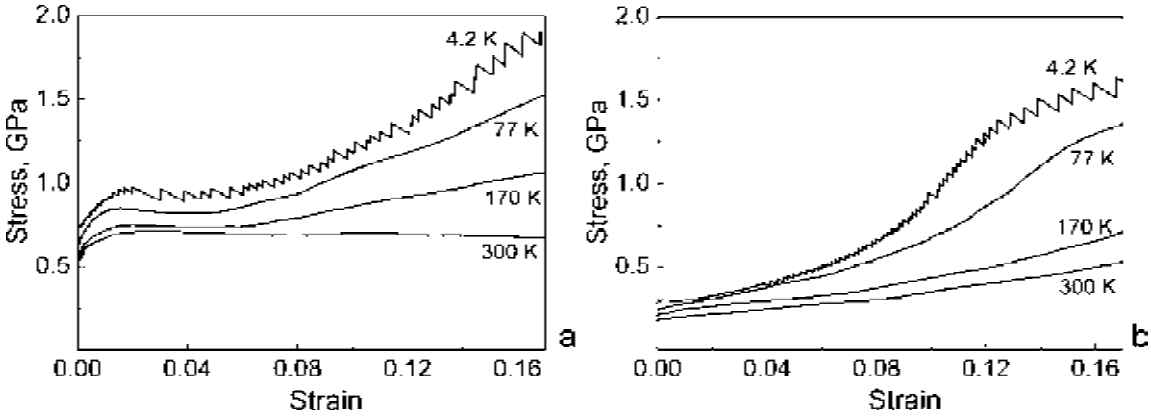

Fig. 3. Typical deformation curves of (a) UFG and (b) CG Zr at temperatures 4.2, 77, 170, and 300K.

Fig. 4. Stage A corresponds to the fast decrease of Θ with strain (ε<0.01-0.04). At stage B (ε>0.01-0.04) Θ considerably increases with strain. At low temperatures (77 and 4.2K) a stage C (decrease of the Θ with strain) can be clearly seen for CG Zr, and possible beginning of stage C is seen for UFG Zr at 4.2K. Changes of the microstructure apparently correspond to the observed stages of Θ(ε) dependence, which will be described in more detail in the next section.

3.3. Evolution of microstructure of the UFG Zr during deformation by compression

Samples of UFG Zr were subjected to several levels of strain (0.02, 0.06, 0.12, 0.18) at different temperatures, and then the microstructure of deformed samples was studied by TEM and X-Ray methods. An example of such microstructure changes can be seen in Fig. 5 for the case of 300K.

The results of the TEM study for the investigated temperatures can be summarized as follows:

- initial UFG Zr shows a microstructure which is typical of that of annealed material: clear and sharp grain boundaries, with interiors of grains being nearly free from dislocation pile-ups, and a low level of internal stresses;
- density of dislocations, dislocation pile-ups, subgrain boundaries increase with strain, but even at a strain of 0.18 their density remain rather small, indicating free passing of a considerable part of dislocations through grains and annihilation of dislocations at grain boundaries, which is typical of UFG materials.

Pole figures (0001) for UFG Zr are presented in Fig. 6, and they show the evolution of texture with

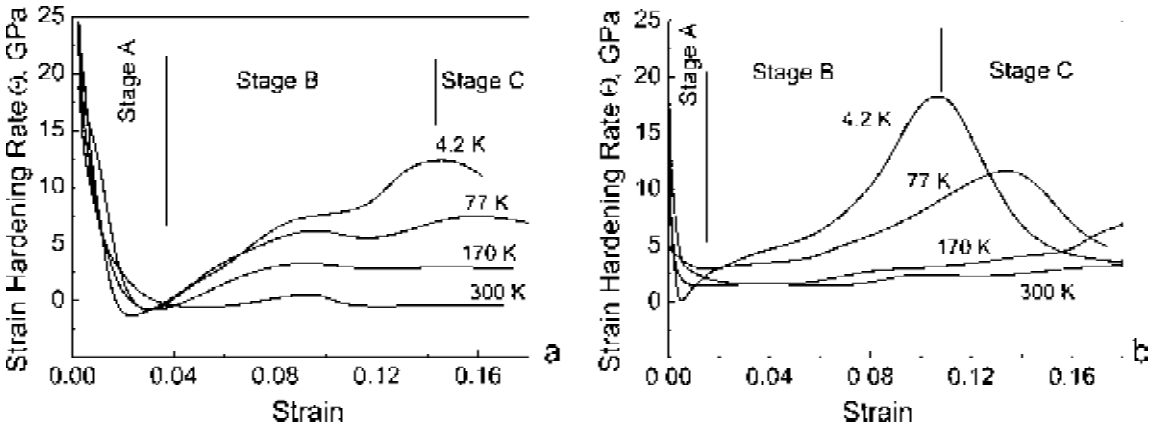

Fig. 4. Strain hardening coefficients at temperatures 300, 170, 77, and 4.2K for (a) UFG Zr and (b) CG Zr; start of stage C is shown for temperature 4.2K.

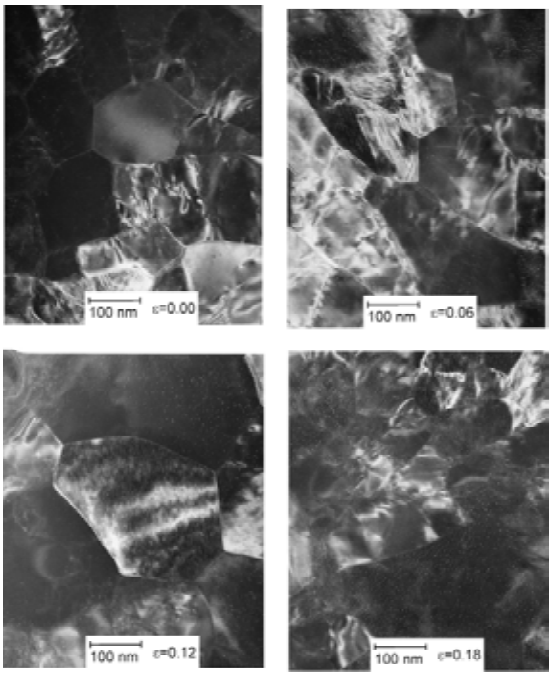

Fig. 5. TEM bright field images for transverse sections of samples of UFG Zr, subjected to compressive strains ε = 0, 0.06, 0.12, and 0.18, at a temperature of 300K.

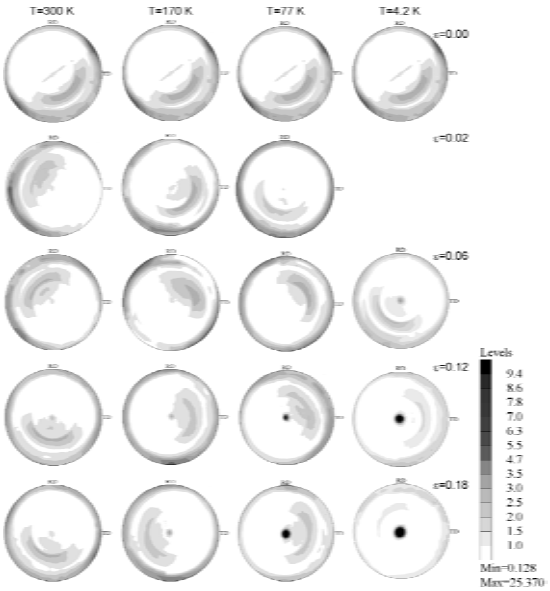

Fig. 6. (0001) pole figures of UFG Zr showing the evolution of texture with increasing compression strain at temperatures 300, 170, 77, and 4.2K (centers of pole figures correspond to the compression direction).

increasing compressive strain at temperatures 300, 170, 77, and 4.2K in UFG Zr. The initial UFG Zr shows a strong c-axis texture in the direction perpendicular to the sample (compression) axis, i.e. the majority of the grains has a c-axis orientation within 90° off the compression direction. Such texture is typical of materials produced by extrusion and wire-drawing. It can be seen from Fig. 6 that straining at a temperature 300K does not lead to any considerable changes of texture, whereas straining at 77 or 4.2K leads to the appearance of an intensity maximum at the center of the pole figures, which corresponds to reorientation of grains to the position with c-axis along the compression axis. At 170K the situation is substantially similar to that of 300K, but a small intensity maximum in the center of the pole figure is also observed at larger strains, which is similar to the low temperature textures. The volume fraction of the reoriented material can be calculated by integration of the orientation distribution function in the limits of the appeared maximum (integration limits were chosen between θ = 0 to 15°, characterizing the deviation from compression axis). Fig. 7a shows the result of this integration – the volume fraction of grains, whose c-axis is oriented between 0 and 15° to the compression axis at different temperatures and strains.

Measurements of the texture were also carried out for initial CG Zr being subjected to strains 0.12 and 0.18 at temperatures 300, 170, 77, 4.2K. The main difference to the UFG case is the absence of the strong c-axis texture in the perpendicular direction to the sample axis. The second peculiarity in CG Zr is that the deformation induced intensity maximum at the center of the (0001) pole figures is broader in comparison to UFG Zr. Accordingly, the volume fraction of the reoriented material in case of CG Zr was calculated by integration of the orientation distribution function with broader integration limits (θ = 0 to 45°) – Fig. 7b.

To find out the reasons of the observed reorientation of grains, the mechanisms of plasticity in Zr are to be analyzed, which is done in the next section.

4. DISCUSSION OF RESULTS

Plasticity mechanisms of CG Zr have been studied in detail at different temperatures [11-15], and the key deformation modes observed at 77K include prismatic slip, two 'tensile' twins, $<10\bar{1}2>$, $<11\bar{2}1>$, and one 'compressive twin', $<11\bar{2}2>$. 'Tensile' and 'compressive' stand for their ability to accommodate tensile and compression strain during defor-

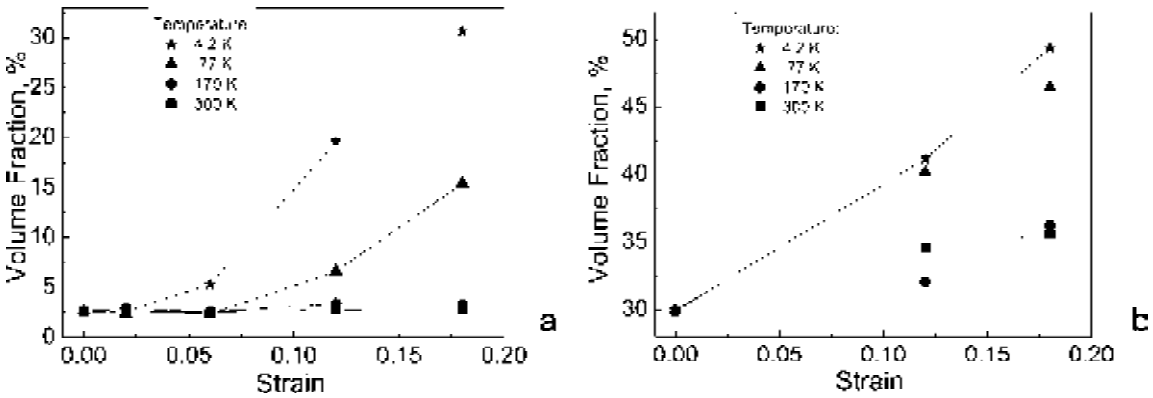

Fig. 7. Variations of volume fraction in (a) UFG Zr, of grains whose c-axis is oriented between 0° and 15° off to the compression axis, and (b) CG Zr, of grains whose c-axis is oriented between 0° and 45° off the compression axis, as a function of deformation temperature and strain (experimental errors are less than the size of points in the plots).

mation in parallel to c-axis. In the case of textured material the activity of the different twinning modes depends on the orientation of deformation axis relative to that of the primary c-axis fiber texture. For compression in parallel to the primary c-axis fiber texture, the dominant deformation mechanisms are first generation compressive <11 $\bar{2}$ 2>twinning and prismatic slip. With further deformation, second-generation tensile twins will also develop; they were proposed to have a significant effect on the evolving microstructure and stress-strain response [13]. For compression perpendicular to the primary c-axis fiber texture (P direction), it was observed that the dominant deformation mechanisms were first generation <10 $\bar{1}$ 2> tensile twinning and prismatic slip. For the case of P direction <10 $\bar{1}$ 2> tensile twinning during compression produces approximately 85° reorientation of the c-axis [13], and it tends to align the c-axis with the compression axis. The evolution of twinned volume fractions like that of <10 $\bar{1}$ 2> tensile twinning can be tracked by recording X-ray or neutron diffraction peak-intensity changes [11,15]; the other possibility of quantitative twin analysis is the direct calculation of twin volume fraction in localized two-dimensional areas by EBSD method. The mentioned methods of twinning analysis were successfully used for twin analysis in coarse grained zirconium [11-15].

In the case of UFG Zr studied in present work, the compression axis is perpendicular to initial c-axis texture (P direction), which has arisen during extrusion and wire drawing, and we observe reorientation processes of grains at approximately 90° to have c-axis aligned along the compression axis (exactly as in the case described above for CG Zr). Thus, it is reasonable to suggest that similar to CG Zr this grain reorientation is caused by the action of <10 $\bar{1}$ 2> twinning. If we subtract the background i.e. the texture intensity of initial UFG Zr, we can determine from Fig. 7a the fraction of reoriented material in the direction of compression axis for different compression temperatures and strains, and identify this fraction of reorientation with that of twin formation. The results of this procedure is presented in Fig. 8a.

The initial state of the CG Zr does not exhibit a strong texture, which means that several different systems of twinning may be active simultaneously, leading to a wide orientation distribution of the reoriented grains. Nevertheless, as in case of the UFG Zr, the twin volume fractions at different temperatures and strains can be associated with the volume fractions of the reoriented material, i.e. the twin volume fractions can be estimated from Fig. 7b by subtracting the value at $\varepsilon = 0$. The results are presented in Fig. 8b. A similar method for the determination of twin volume fraction for CG zirconium being strained at 77K, was successfully applied within a neutron diffraction texture study [15].

The estimated twin volume fractions for CG Zr (Fig. 8b) can be compared with the literature data: In paper [13] for the case of compression of the high purity CG Zr at temperature 77K, the twin volume fractions were estimated by means of EBSD as 17% at a strain of 0.12, and 45% at a strain of 0.18; in paper [15], the twin volume fraction amounted to approximately 20% at a compressive strain of 0.12 at 77K for high purity CG Zr. In the present

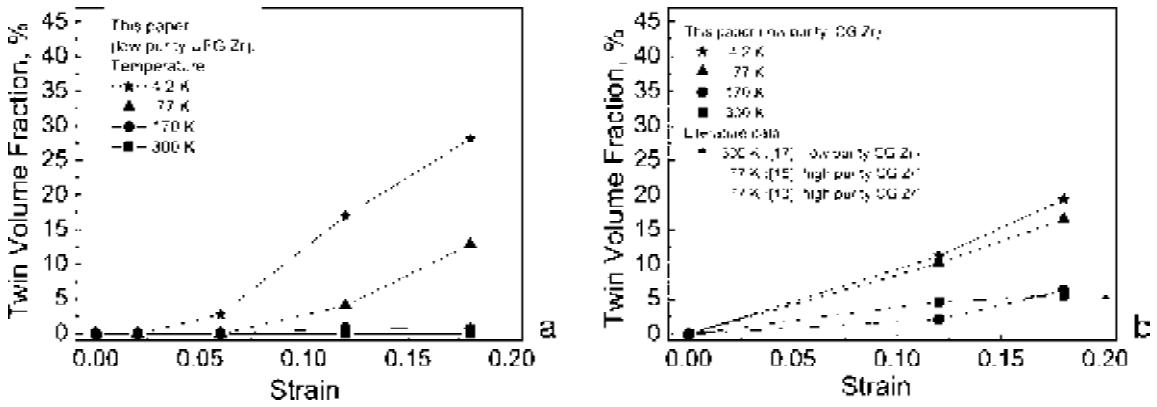

Fig. 8. Evolution with strain of twin volume fraction of (a) UFG Zr ; and (b) CG Zr at temperatures 4.2, 77, 170, and 300K (experimental errors are less than the size of points in the plots). In Fig. 8b literature data for CG Zr are also shown.

work, we studied low purity Zr and the activity of twinning in CG Zr at 77K is approximately two times lower than the mentioned literature data for the corresponding temperature and compression strain of high purity CG Zr. This smaller value of twin density in low purity CG Zr is consistent with results of work [16], where it has been reported that the activity of twinning in Zr decreases with increasing concentration of interstitial impurities. An estimation of the twin volume fraction gives 5% in CG low purity Zr [17] at 300K after compression of 0.2, which is in good agreement with our data (Fig. 8b).

It can be seen from Fig. 8 that twinning is active in CG Zr at all temperatures studied. However, while the transition from 170 to 77K leads to a considerable increase of twinning activity, another decrease of temperature to 4.2K practically does not achieve a further growth of twinning activity. The situation in UFG Zr is strongly different: twinning is completely absent at 300K, but at 170K its activity is still very small, whereas at 77K the twin fraction comes close to that of compressed CG Zr, and at 4.2K the activity of twinning even *exceeds* the corresponding value for CG at 4.2K. It was suggested in paper [18] that the activity of twinning should decrease with decreasing grain size, and this result has widely spread in the community [3,13]. Comparing our findings in UFG and CG Zr, these confirm this result for compression temperature 300K and 170K. However, at the temperature 77K the activity of twinning is approximately the same in both cases, and then at 4.2 K, there occurs an inverse effect: the activity of twinning is *higher* in UFG Zr than in CG Zr.

It is interesting to note that such an inverse (Hall-Petch type) effect of twinning has been reported recently for fcc nanometals [19]; however, with the present work, such an effect is shown for the first time for hcp nanometals, and another new finding is that the deformation temperature plays an important role for that effect.

Twinning is known to be the main reason of strain hardening increase during low temperature compressive straining of coarse grained hcp metals (Zr [11] and Ti [10]). The strain hardening arises from the twin boundaries acting as additional barriers for dislocation motion. In our case, the active twin system reorients grains to a position which is not favourable for dislocation gliding, and thus leads to additional strain hardening. In sum, the strain hardening behavior observed of CG and UFG Zr (Figs. 3 and 4) can be described as follows: (i) at all deformation temperatures, strains and structural states studied, Zr shows active prismatic slip of dislocations which takes a considerable part of plastic deformation; (ii) at stage A of strain hardening curve, plasticity and strain hardening is controlled by prismatic slip of dislocation only; (iii) the onset of the stage B (increasing of strengthening) corresponds to the beginning of considerable twinning: increases of twin volume fractions (Fig. 8) correspond to increases of the strain hardening characteristics (Fig. 4), at 300K in UFG Zr, however, twinning is not active and stage B is not observed, (iiii) the decrease of strain hardening (stage C), observed at low temperatures, corresponds to saturation of twinning activity [10], and in CG Zr this process sets in at lower strains than in UFG Zr (Fig. 4).

5. SUMMARY AND CONCLUSIONS

The results of this work and their interpretations done on CG and UFG Zr can be summarized as follows:

- the combination of extrusion, wire drawing and annealing allows to produce an UFG structure in Zr with average grain sizes of 0.2 μm, whose strength exceeds the strength of CG Zr (grain size ~ 10 μm) by 2.5-3 times in a wide range of low temperatures. At the same time, plasticity remains considerable;
- prismatic slip of dislocation and twinning are the main mechanisms which rule the plasticity in UFG Zr. The activity of twinning is smaller in UFG Zr in comparison with CG Zr at ambient and lower deformation temperatures, but is markedly higher for very low temperatures (4.2K): here, twinning *increases* with decreasing grain size;
- twinning governs the observed strain hardening increase of UFG Zr at low temperatures in deformation stage B.

ACKNOWLEDGEMENTS

This work has been carried out with financial support by the scientific technical cooperation project Austria-Ukraine M/64-2009 (UA 15/2009) and by project 1/09-NANO of the National Academy of Sciences of Ukraine complex program “Nanosystems, nanomaterials and nanotechnologies”.

REFERENCES

[1] R. Z. Valiev, Y. Estrin, Z. Horita, T. G. Langdon, M. J. Zehetbauer and Y. T. Zhu // *JOM*, April (2006) 33.

[2] V. V. Stolyarov, Y. T. Zhu, I. V. Alexandrov, T. C. Lowe and R. Z. Valiev // *Materials Science and Engineering* **A299** (2001) 59.

[3] G.G. Yapici and I. Karaman // *Materials Science and Engineering* **A 503** (2009) 78.

[4] L. Jiang, M.T. Perez-Prado, P.A. Gruber, E. Arzt, O.A. Ruano and M.E. Kassner // *Acta Materialia* **56** (2008) 1228.

[5] M.A. Meyers, A. Mishra and D.J. Benson // *Progress in Materials Science* **51** (2006) 427.

[6] E.D. Tabachnikova, V.Z. Bengus, A.V. Podolskiy, S.N. Smirnov, V.D. Natsik, K. Csach, J. Miskuf, D.V. Gunderov and R. Valiev // *Reviews on Advanced Materials Science* **10** (2005) 229.

[7] E. D. Tabachnikova, A. V. Podolskiy, V. Z. Bengus, S. N. Smirnov, and V. D. Natsik, V. M. Azhazha, M. A. Tikhonovskiy, A. N. Velikodny, N. F. Andrievskaya, G. E. Storozhilov and T. M. Tikhonovskaya // *Low Temperature Physics* **34** (2008) 969.

[8] P. Van Houtte // *Textures and Microstr.* **13** (1991) 199.

[9] K. Pawlik and P. Ozga, *LaboTex: The Texture Analysis Software, Głttinger Arbeiten zur Geologie und Paläontologie, SB4* (1999).

[10] A. A. Salem, S. R. Kalidindi, R. D. Doherty and S. L. Semiatin // *Metallurgical and Materials Transactions A* **37** (2006) 259.

[11] G. Kaschner, C. Tome, I. Beyerlein, S. Vogel, D. Brown and R. McCabe // *Acta Materialia* **54** (2006) 2887.

[12] R.E. Reed-Hill, In: *Deformation Twinning*, ed. by R.E. Reed-Hill, J.P. Hirth and H.C. Rogers (TMS, Warrendale, PA, 1964) vol. 25, p. 295.

[13] R.J. McCabe, G. Proust, E.K. Cerreta and A. Misra // *International Journal of Plasticity* **25** (2009) 454.

[14] D. Bhattacharyya, E.K. Cerreta, R. McCabe, M. Niewczas, G.T. Gray III, A. Misra and C.N. Tome // *Acta Materialia* **57** (2009) 305.

[15] P. Rangaswamy, M.A.M. Bourke, D.W. Brown, G.C. Kaschner, R.B. Rogge, M.G. Stout and C.N. Tome // *Metall. Mater. Trans. A* **33A** (2002) 757.

[16] G.C. Kaschner and G. T. Gray III // *Metall. Mater. Trans. A*, **31A** (2000) 1997.

[17] O. Castelnau, H. Francillette, B. Bacroix and R.A. Lebensohn// *Journal of Nuclear Materials* **297** (2001) 14.

[18] S. G. Song and G. T. Gray III // *ACM metall. mater.* **43** (1995) 2339.

[19] X.L.Wu and Y.T.Zhu // *Phys.Rev.Lett.* **101** (2008) 025503.